On the Evolution of the *QE II* Storm. II: Dynamic and Thermodynamic Structure

JOHN R. GYAKUM[1]

Department of Meteorology and Physical Oceanography, Massachusetts Institute of Technology, Cambridge, MA 02139

(Manuscript received 21 June 1982, in final form 26 October 1982)

ABSTRACT

The existence of convection and the hurricane-like structure in the explosively-developing cyclone studied in Part I motivates us to assess the importance heating had on this cyclogenesis. To accomplish this, a method to evaluate the three-dimensional thermodynamic and dynamic structure of the atmosphere is proposed, so that we may evaluate potential vorticity changes in the vicinity of this cyclone. Results indicate a 24 h lower tropospheric generation of from five to thirteen times the value observed at 1200 GMT 9 September 1978.

An evaluation of physical effects on thickness change following the surface center shows a large mean tropospheric temperature rise to be due to bulk cumulus heating effects, which could be important in the extraordinary potential vorticity generation concurrent with this cyclone's explosive development.

These vertically integrated values of heating motivate us to solve the quasi-geostrophic omega and vorticity equations forced by an idealized heating function with specified horizontal scale, level of maximum heating and total heating. Resulting theoretical omega profiles and height falls during the 24 h period of explosive development for the observed integrated values of heating, vorticity–stability parameter, and over a wide range of levels of maximum heating readily account for the observed explosive cyclogenesis. It is hypothesized that the relatively weak baroclinic forcing operative in this case helped to organize the convective bulk heating effects on a scale comparable to the cyclone itself in an atmosphere which is gravitationally stable for large-scale motions and gravitationally unstable for the convective scale. This CISK-like mechanism, evidently operative in this case, is further hypothesized to be important in other explosively-developing extratropical cyclones, just as it is generally regarded to be crucial in tropical cyclone development.

1. Introduction

This paper represents Part II of the study of the explosively-developing cyclone which battered the liner *Queen Elizabeth II* in September 1978. As a follow-up to the synoptic conditions presented by Gyakum (1983, hereafter referred to as I), this paper's purpose is to assess quantitatively the role cumulus-induced heating had on the cyclogenesis. The fact that this cyclone had hurricane-like characteristics in the wind and cloud fields makes this hypothesis deserving of further study.

The debate over whether cyclones occurring in extratropical regions are fundamentally driven by baroclinic or by convective processes has continued over the past several years. Tracton (1973) has presented evidence for convective processes triggering cyclogenesis in a series of continental cases. Harrold and Browning (1969) and Mansfield (1974) studied cyclones in cold air outbreaks (polar lows), and concluded they are well-understood shallow baroclinic disturbances. However, Reed (1979) has further argued that Conditional Instability of the Second Kind (CISK, as proposed by Charney and Eliassen, 1964) may also play an important role in these disturbances. Rasmussen (1979), in fact, has suggested that the polar low is fundamentally a CISK phenomenon, just as tropical cyclones have been hypothesized to be. Furthermore, Bosart (1981) has shown the President's Day (February 1979) cyclone's rapid intensification to have been associated with deep convection near its clear, eyelike center.

This paper examines the effects of heating upon this cyclogenesis with a potential vorticity analysis. In order to accomplish this, a procedure to find the three-dimensional thermodynamic structure of the atmosphere is discussed and applied to this case in Section 2. An examination of the potential vorticity fields associated with this cyclone is performed in Section 3, with the goal of assessing quantitatively the importance of heating and frictional effects. A discussion of probable diabatic effects and their influence on the potential vorticity changes is contained in Section 4. Section 5 utilizes a simple diagnostic model to examine the dynamical consequences of the vertically-integrated heating found in Section 4. The observational and theoretical results of this paper provide a basis for a development hypothesis in Section 5 and the conclusions in Section 6.

[1] Current affiliation: Department of Atmospheric Sciences, University of Illinois, Urbana, IL 61801.

2. Thermodynamic structure

Although we have little information on the detailed three-dimensional temperature and moisture structure around this rapidly developing cyclone, good ship and Seasat surface coverage exists along with a substantial number of commercial aircraft reports at approximately 250 mb. Vertical profiles of virtual temperature were constructed from this information on a one degree latitude by one degree longitude grid surrounding the surface cyclone for 1200 GMT 9 and 10 September. The information given for each grid point includes sea level pressure, surface temperature, dew point temperature, 1000–250 mb thickness, instrument elevation, 250 mb temperature, and the tropopause level.

Computing a virtual temperature profile involves a given thickness in the layer from pressure P_1 to P_2 specifying the mean layer virtual temperature $\bar{T}_v$:

$$\bar{T}_v = \int_{P_2}^{P_1} T_v(P) d \ln P \left[\int_{P_2}^{P_1} d \ln P \right]^{-1}. \quad (1)$$

To solve for the numerator on the right side of (1), we use the observed virtual temperature at the bottom boundary, along with an assumed vertical variation of the virtual temperature of the form

$$T_v(P) = T_B(P/P_B)^{\text{slope}}, \quad (2)$$

where T_B is the virtual temperature at pressure P_B, the lower boundary reference level. Slope is defined as $\ln[T_v(P)/T_B]/\ln(P/P_B)$. By substituting (2) into (1), we may solve iteratively for slope to any desired accuracy, for this study 1.5×10^{-4}. This procedure will provide a 1000–250 mb temperature structure that will hydrostatically yield a thickness to within 0.5 m of the order 10^4 m input 1000–250 mb thickness. Note that slope = 0.288 and 0.0 represent dry-adiabatic and isothermal lapse rates, respectively.

Surface temperatures, 1000–250 mb thicknesses and 250 mb temperatures were included as input to the algorithm, so that two slopes are computed for each grid point, with the transition point between the two lines chosen as the tropopause level P_T, where $P_T > 250$ mb, and an arbitrary choice made for this transition level, P_{tr}, where $P_T \leq 250$ mb. The 250 mb temperature and tropopause fields within the computational domains, are shown in Fig. 1. Note the relatively high tropopause height, characteristic of the subtropics, over the surface center at both times. The virtual temperature for each gridpoint is given by

$$T_v(P) = T_B(P/P_B)^{\text{slope 1}}, \qquad P_{tr} \leq P \leq P_B, \quad (2a)$$

$$T_v(P) = T_{tr}(P/P_{tr})^{\text{slope 2}}, \quad 250 \text{ mb} \leq P \leq P_{tr}. \quad (2b)$$

Slope 1 and slope 2 are constrained to be ≤ 0.288 (lapse rate is not to exceed dry adiabatic). Computations were performed for many transition levels, and the sensitivity of the results to the choices will be discussed.

Fig. 2 compares model temperature profiles with observed virtual temperature profiles at nearby radiosonde stations. The mean virtual temperature of the observed and model soundings is the same, except for the small difference in thickness brought about by the displacement of the grid point from the radiosonde station. At Caribou where the tropopause is just above 400 mb, temperature errors of a fraction of a degree Celsius exist up to tropopause level, and 2–3°C above the tropopause where the temperature profile contains many changes in slope at 10–15 mb intervals. The Portland sounding, with its tropopause at 207 mb, allows us to experiment with different transition points in the model soundings. Temperature differences among the two model soundings are on the order of a fraction of a degree, and never exceed 1°C. The primary error occurs in the region of the observed inversion above 640 mb. Although temperature error magnitudes approach 2°C through much of the sounding, model lapse rates are within 20% of the observed rate, except for the 30 mb layers near the surface and 650 mb. This example merely shows the inherent limitations of the procedure due to lack of intermediate-level temperature information. However, our method will reasonably compute static stabilities for layers of depth 100 mb or more.

Constructed soundings over the storm center for 1200 GMT 9 and 10 September are shown in Fig. 3. Although the most uncertainty in the virtual temperature profiles is in the lower troposphere, all six soundings indicate the atmosphere to be absolutely stable, with the more stable atmosphere indicated at 1200 GMT 10 September. At this time, the 400 mb transition sounding is in error, for the computed 250 mb temperature is 5.5°C higher than observed as a result of the algorithm not computing lapse rates greater than dry adiabatic. The dashed line represents the "correct" (but super-adiabatic) upper part of this sounding. The intermediate-level aircraft temperature observations taken in the vicinity of the low center show the two lower transition point soundings to be more correct. Thus, the strong lower tropospheric static stability seems confirmed at this time.

Though absolute static stability exists over the surface center at 1200 GMT 9 September, potential instability at this time is widespread over the storm domain. The Chatham (90 km north-northeast of the center) sounding (Fig. 4) shows the stable 1000–800 mb temperature stratification, but also the equivalent potential temperature (θ_e) decreases 12°C in this layer. This 2 km layer of potentially unstable air is supported by the satellite images (Fig. 15 of I) which indicate convective cloud tops at the 750–800 mb levels near the storm center. Clearly, the lower tropospheric upward motion found quasi-geostrophically (Fig. 21 of I) and observationally (Fig. 19 of I)

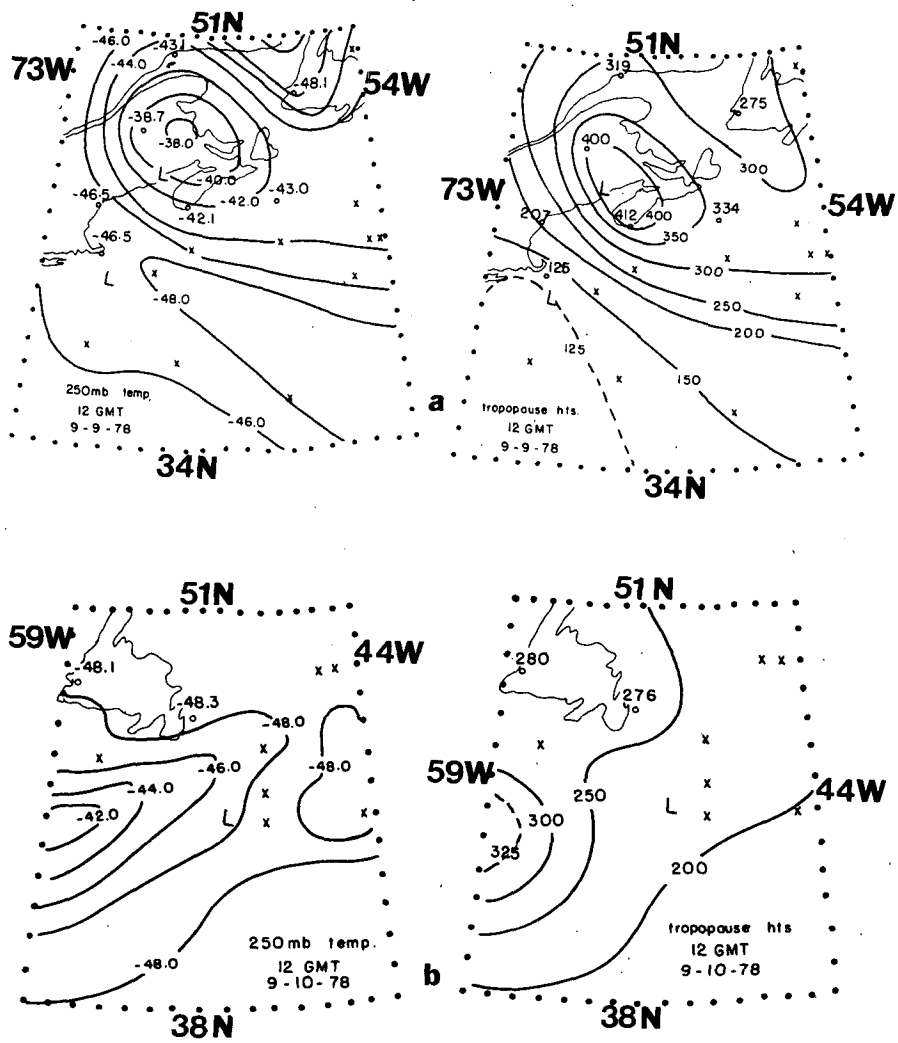

FIG. 1. Tropopause and 250 mb temperature analyses for 1200 GMT (a) 9 and (b) 10 September. Circles indicate radiosonde data points, and ×'s indicate locations of commercial aircraft observations. "L" indicates the position of the surface cyclone center. Dots show the boundary of the computational domain. Tropopause heights are expressed in mb.

is sufficient to destabilize the potentially unstable atmosphere. The resulting lower tropospheric static instability thus provides a favorable environment for the observed shallow convective elements over and to the east of the center at this time.

A more expansive (but less accurate) view of the stratification at this time is shown in the model-derived θ_e profiles for the 69 and 59°W cross sections in Fig. 5. These profiles were derived using the model virtual temperature profiles as a function of pressure and, assuming saturation, the resulting saturation mixing ratios. The profile through the storm center shows an increasingly deep potentially unstable layer extending southward from the center to 550 mb at 34°N. Perhaps more important for the evolution of this shallow storm is the potentially unstable air which exists through increasingly deep layers eastward of the storm center, as shown in the 59°W cross section. Potential instability exists throughout its meridional extent and up to 700 mb over the grid point at which the storm will arrive ~10 h hence. This fact is consistent with the decreasing tropospheric thicknesses eastward from the center over the relatively uniform sea surface temperatures (Figs. 9 and 10 of I), and helps to account for the much deeper convective towers observed later in the cyclone evolution (Fig. 15 of I).

3. Potential vorticity fields

This section quantitatively assesses the importance of the diabatic and frictional effects associated with this extraordinary cyclone. This is accomplished with an evaluation of potential vorticity. Ertel (1942) has

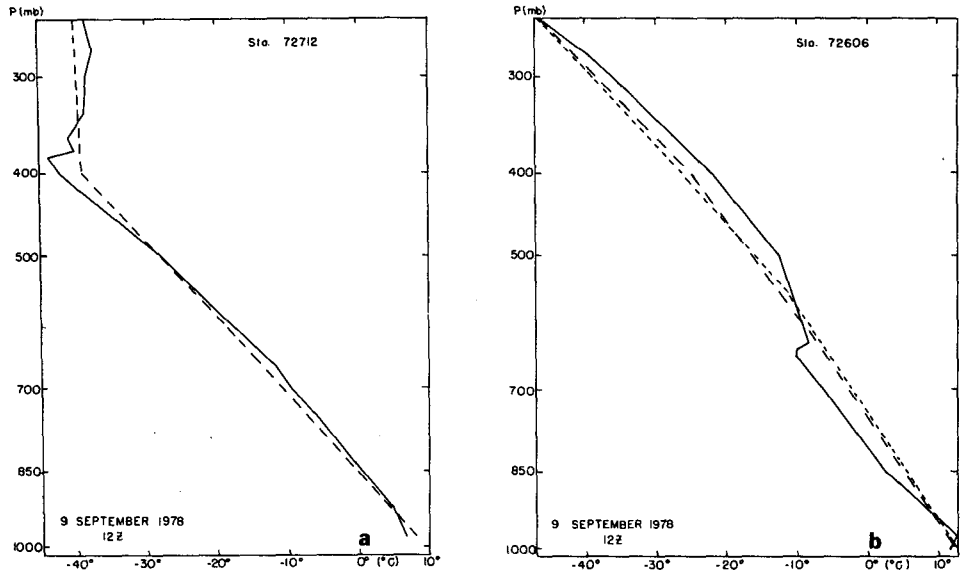

FIG. 2. (a) Virtual temperature structure for station 72712 (Caribou, Maine) for 1200 GMT 9 September is indicated by the solid line. Dashed line is the model virtual temperature profile for the same time at the nearest grid point (47°N, 68°W). (b) As for (a), except for station 72606 (Portland, Maine) and the grid point 44°N, 70°W. Short dashed line indicates model temperatures with transition level of 550 mb, and long dashed line shows the model profile with 400 mb transition point.

shown that potential vorticity Q is conserved for frictionless, adiabatic motion, i.e.,

$$dQ/dt = 0, \tag{3}$$

where t is time, $Q = (\omega \cdot \nabla\eta)/\rho$, ω is the absolute vorticity vector, η is the function of state and ρ is the density. If we assume potential temperature θ to be the function of state, note that θ changes most rapidly in the vertical, and use the hydrostatic relation, (3) reduces to

$$d/dt[-g(\partial\theta/\partial P)(\zeta_\theta + f)] = 0, \tag{3a}$$

where g is the gravitational acceleration, f the Coriolis parameter, and ζ_θ the relative vorticity evaluated on a θ surface.

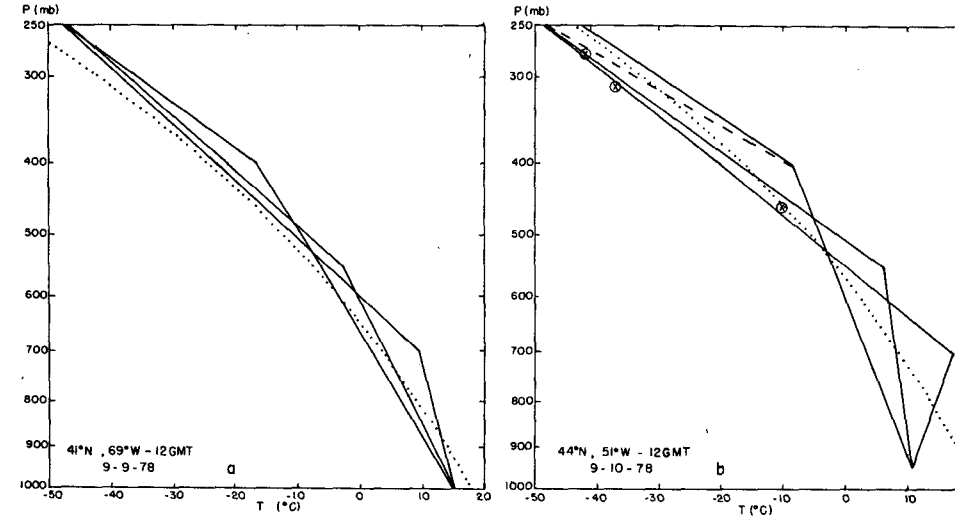

FIG. 3. (a) Soundings at grid point 41°N, 69°W for 1200 GMT 9 September for transition points at 700, 550, and 400 mb. Dotted line is representative moist adiabat. (b) As for (a), except for grid point 44°N, 51°W at 1200 GMT 10 September. Aircraft temperature observations within 200 km of the cyclone center are shown by circled X's.

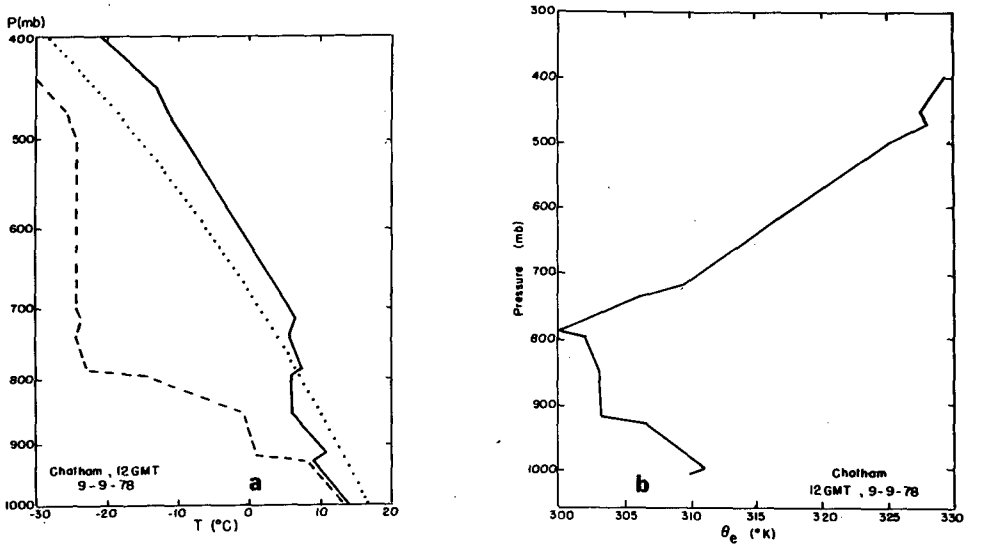

FIG. 4. (a) Chatham sounding for 1200 GMT 9 September 1978 of temperature (solid line), and dewpoint temperature (dashed line). The 321 K saturation equivalent-potential temperature isotherm is the dotted line. (b) As for (a), except for the equivalent potential temperature.

Gravity-weighted profiles of potential vorticity have been computed for this case in the following manner. The θ profiles for each grid point are constructed according to the procedure outlined in the previous section. Vertical differences of θ are computed over a finite-difference interval of 30 mb. The relative vorticity on a θ surface is evaluated over a horizontal finite difference interval of one degree latitude in the north–south direction, and one degree longitude in the east–west direction. The winds on which the relative vorticity computations are based are computed for each grid point each 15 mb from the surface to 250 mb, and then interpolated onto the appropriate θ surface. The thermodynamic structure found within the cyclone domain hydrostatically specifies geopotential heights for any desired pressure level up to 250 mb. These fields allow the computation of geostrophic winds, which are modified to take into account viscous forces in the planetary boundary layer (assumed 1000 m in depth) with the classical Ekman spiral solutions. Because of the strong cyclonic curvature present in this case, the geostrophic wind speed is an overestimate of the actual wind speed. The more accurate gradient wind estimate, specified by the geostrophic wind speed and by the radius of the parcel trajectory R_t, is thus used for all potential vorticity computations. The trajec-

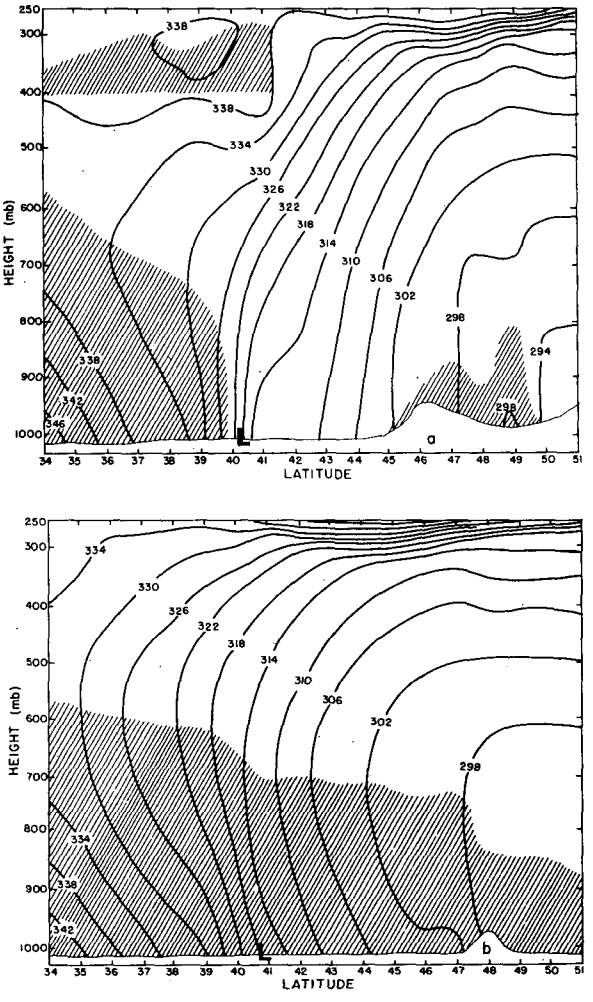

FIG. 5. (a) Meridional profiles of equivalent potential temperature (constructed for transition level 400 mb) for 1200 GMT 9 September 1978 for 69°W. Shaded regions indicate a decrease of θ_e with height. Light solid line shows the earth's surface. Location of surface cyclone is indicated with an "L." (b) As for (a), except for the 59° cross section. "L" indicates eventual position of the surface cyclone in this section.

tory radius was calculated using the streamline radius R_s (approximated by the curvature radius of the geopotential height field), and the instantaneous velocity c of the surface low. Thus,

$$R_t = R_s \Big/ \left(1 - \frac{|c|}{V}\cos\alpha\right)$$

(Holton, 1972, p. 47), where V is approximated by the geostrophic wind speed, and α is the angle between the streamline (isobar) and the direction of surface system movement.

Several experiments with the potential vorticity computation were performed for 1200 GMT 9 and 10 September—both times for which we have a good knowledge of the sea-level pressure and tropospheric thickness fields. Figs. 6 and 7 show meridional cross sections through the storm center of potential vorticity and the θ surfaces on which they are computed. The figure clearly shows substantial potential vorticity gain following the center during the 24 h period beginning 1200 GMT 9 September. This result is insensitive to the choice of transition level, though the vertical extent of the large potential vorticity values is uncertain. We may use this set of charts for each time as specifying the range of uncertainty of our calculations. Thus, 100 mb above the surface center on the 9th, we have calculated potential vorticities ranging from 1.1 to 1.7 ($\times 10^{-5}$) s^{-1} K mb^{-1}, and for the 10th, values range from 8.0 to 14.0 ($\times 10^{-5}$) s^{-1} K mb^{-1}. An inspection of the computed gradient wind fields in the lower troposphere above the surface center at 1200 GMT on the 10th reveals maximum wind speeds of 50 m s^{-1}, which are consistent with

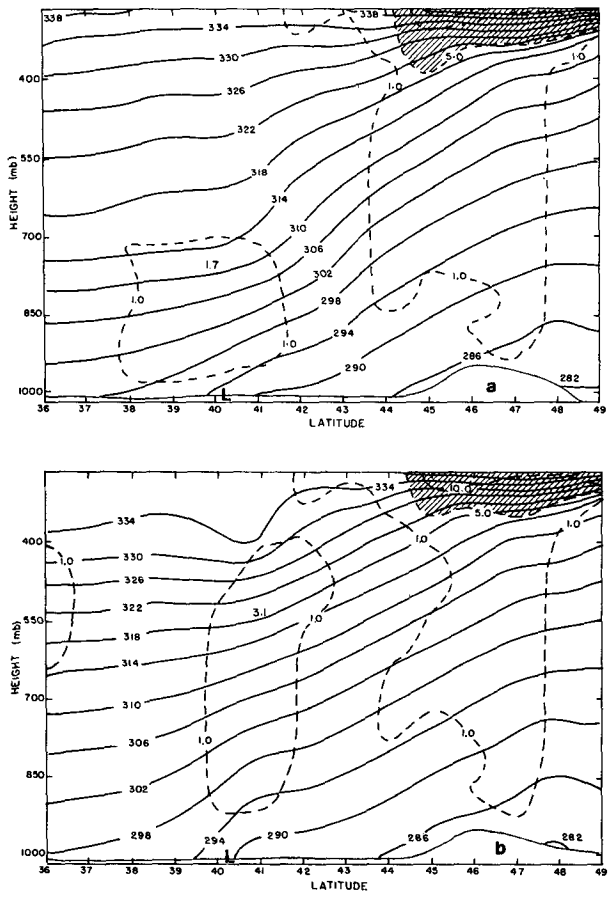

FIG. 6. Meridional cross sections of potential vorticity ($-\partial\theta/\partial P)(\zeta_\theta + f)$, with units of 10^{-5} K mb^{-1} s^{-1}, and potential temperature (θ) in K for longitude 69°W at 1200 GMT 9 September 1978. Light solid line indicates the earth's surface. Transition levels are (a) 700 mb and (b) 400 mb. Surface cyclone position is shown with an "L."

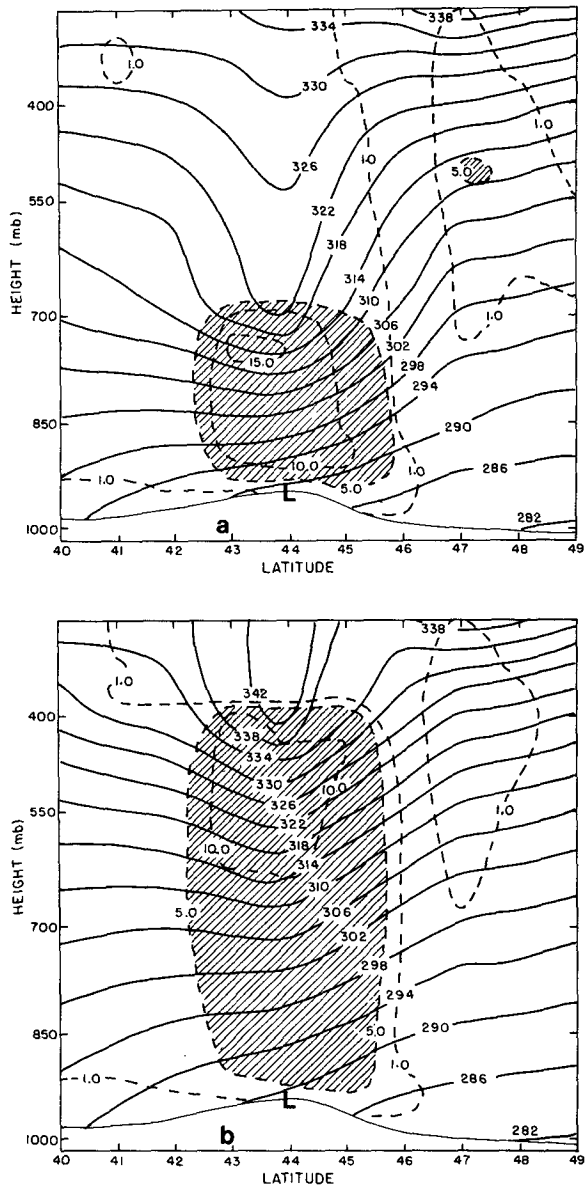

FIG. 7. As in Fig. 6, except for longitude 51°W at 1200 GMT 10 September.

the observed speeds near the surface of 30–35 m s^{-1}. Thus, it appears the maximum error in this computation is about 20% of 50 m s^{-1}. Fluctuations of this magnitude in the computed gradient winds imply a corresponding 20% error in the computation of the isentropic relative vorticity. This is well within the range of typical potential vorticity values just described for 1200 GMT 10 September. The range of possible lower tropospheric static stabilities and isentropic slopes has already been accounted for in the former computations. A similar error bound is found for the wind fields at 1200 GMT 9 September.

Our objective is to estimate possible sources of potential vorticity to account for the strong generation found above. As has been shown by Staley (1960) and Gidel and Shapiro (1979), among others, the expression for the time rate of change of potential vorticity is

$$dQ/dt = g\omega \cdot \nabla\dot{\theta} - g(\partial\theta/\partial P)\mathbf{k} \cdot \nabla_\theta \times \mathbf{F}, \quad (4)$$

where $\nabla\dot{\theta}$ is the gradient of diabatic temperature change, $\mathbf{k}$ is the vertical unit vector, ∇_θ is the gradient operator along a constant θ surface, and $\mathbf{F}$ is the force per unit mass produced by turbulent stresses. The first term on the right of (4) is the diabatic source term, and the second term is the frictional effect on potential vorticity. Each term may be expanded as follows:

$$g\omega \cdot \nabla\dot{\theta} = -g\left[(\zeta_\theta + f)\frac{\partial\dot{\theta}}{\partial P} + \frac{\partial\theta}{\partial P}\left(\zeta_x\frac{\partial\dot{\theta}}{\partial x} + \zeta_y\frac{\partial\dot{\theta}}{\partial y}\right)\right], \quad (4a)$$

$$-g\frac{\partial\theta}{\partial P}\mathbf{k} \cdot \nabla_\theta \times \mathbf{F} = (-g\partial\theta/\partial P)\left[\frac{\partial}{\partial x}\left(\frac{\partial\overline{\omega'v'}}{\partial P}\right) - \frac{\partial}{\partial y}\left(\frac{-\partial\overline{\omega'u'}}{\partial P}\right)\right], \quad (4b)$$

where $\zeta_x = \partial v/\partial\theta$ (v is the north–south wind), $\zeta_y = \partial u/\partial\theta$ (u is the east–west wind), the bar is a time average at a fixed point throughout some characteristic turbulent scale, and the prime represents a turbulent deviation from the time average. Gidel and Shapiro have described the first term on the right of (4a) as the stability change term and the second term as the vorticity tilting term. The potential importance of this latter term may be evaluated by estimating each component as follows: $\partial\theta/\partial P \sim 1$ K $(10\text{ mb})^{-1}$, $\zeta_x \sim 1$ m $(\text{s K})^{-1}$. The large-scale condensational heating taken from the storm-scale ascent found in I at 1200 GMT 10 September varies over a 10^3 km horizontal interval. Thus $\partial\dot{\theta}/\partial x \sim 10^4$ ergs gm^{-1} s^{-1}/(10^6 m), and an order O[10^{-6} K s^{-1} mb^{-1} (12 h)$^{-1}$] term is found, which is a small contribution. However, if this heating varied over a 10^2 km distance, or if the observed cumulus convection affected additional organized heating fields, this tilting term could become a significant negative or positive factor in the storm-scale potential vorticity budget.

Instantaneous evaluations of the first term on the right of (4a) for 1200 GMT on the 9th and 10th have each been extrapolated 12 h to yield an estimate of the 24 h potential vorticity change. The storm-scale vertical motions (from I) and the computed thermal stratifications at these times, are used to compute vertical distributions of storm-scale condensational heating. This information, with estimates of the vertical component of the absolute vorticity, yields an estimated potential vorticity generation of O(10^{-4} K s^{-1} mb^{-1}), which is strong enough to account for the observed increase, if we had actually observed this static stability increase. However, such a dramatic static stability increase is not found, and the shortfall is compensated for by the three to four-fold increase in relative vorticity observed in this system. Since this term only accounts for the static stability change, we may conclude that if heating is primarily responsible for the observed dramatic potential vorticity increases, the above "tilting" term is responsible in the manner discussed above.

The frictional effect on potential vorticity (4b) shows that changes in ζ_θ can result from horizontal gradients of the vertical divergence of the turbulent momentum flux. This effect's magnitude is proportional to the static stability. We will now obtain an estimate of this effect's potential importance. The maximum updraft speeds in the cumulus towers are of O(10 m s^{-1}), while the perturbation horizontal speeds are also 10 m s^{-1}. Assuming this turbulent momentum flux occurs over a depth of some 4 km, this vertical momentum flux divergence is O(10^{-2} m s^{-2}). If the horizontal change of this quantity occurs over O(100 km) distance, and the tropospheric increase of θ with height is O(1 K/10 mb), then the 12 h potential vorticity change is O(10^{-4} K mb^{-1} s^{-1}). This is a potentially large effect, though its persistence over such a long time is doubtful. The sign of this term depends upon the location and character of the convection with respect to the computational point.

Though the data are not sufficient to estimate this "cumulus friction" effect, its import in explaining the large 24 h potential vorticity increase is likely small. Thus, the remainder of this paper will be devoted to a discussion of diabatic warming, whose effect we can reasonably estimate. An evaluation of this warming will determine whether cumulus friction is needed to explain the observed potential vorticity increase.

4. Diabatic effects

A clue to the extent of the diabatic influence may be gained from an examination of mean tropospheric temperature changes observed over the storm center. As shown in I, there is a dramatic (8°C) jump in the column-mean temperature over the center from 0000

GMT to 1200 GMT 10 September. Whereas the potential vorticity change is a function of how heating is vertically and horizontally distributed, and these heating distributions are not easily observed, the thickness change following the center is a means by which we may diagnose the much stronger signal of the integrated diabatic effects.

We may evaluate the known physical effects on the thickness change following the low center by using the following technique, which is based upon the analysis of Sanders (1976). We first express the thermodynamic energy equation as

$$\frac{\partial h}{\partial t} = -\mathbf{v}\cdot\nabla h + \left(\frac{\partial h}{\partial t}\right)_{\text{adi}} + \left(\frac{\partial h}{\partial t}\right)_{\text{dia}}, \qquad (5)$$

where $\partial h/\partial t$ is the local thickness (h) change rate (for the 1000–250 mb layer in this case), $-\mathbf{v}\cdot\nabla h$ is the vertically-integrated horizontal temperature advection effect. The last two terms consist of the thickness change due to adiabatic warming and cooling associated with storm-scale vertical motions $(\partial h/\partial t)_{\text{adi}}$, and of all diabatic effects $(\partial h/\partial t)_{\text{dia}}$, except for large-scale pseudo-adiabatic processes, which will be incorporated into $(\partial h/\partial t)_{\text{adi}}$.

This adiabatic term may be expressed in terms of the vertical motion and the stratification by noting $\partial h/\partial t = \partial/\partial t \int_{1000}^{250} (\partial z/\partial P)dP$, and $\partial\theta/\partial t = -\omega\partial\theta/\partial P$, where ω is the vertical motion, and θ the potential temperature. Thus, the equation of state, hydrostatic assumption, and Poisson's equation combine to yield

$$\left(\frac{\partial h}{\partial t}\right)_{\text{adi}} = -\int_{250}^{1000}\left[\frac{(RT\omega)}{(g\theta)}\right]\left(\frac{\partial\theta}{\partial P}\right)d\ln P. \qquad (6)$$

With our knowledge of the stratification over the storm center (Section 2) and the parabolic profile of ω (described in I) we may integrate (6). We will take account of latent heat release in saturated rising-air by the replacement of $\partial\theta/\partial P$ in (6) with $[\partial\theta/\partial P - (\partial\theta/\partial P)_{\text{ma}}]$, where $(\partial\theta/\partial P)_{\text{ma}}$ is the change of potential temperature along the appropriate moist adiabat.

The thickness change following the center may be expressed as the sum of the three physical effects in (5) plus the effect of cyclone movement (at velocity $\mathbf{c}$) to air of different mean temperature, $\mathbf{c}\cdot\nabla h$. Thus, (5) becomes

$$\left(\frac{\partial h}{\partial t}\right)' = \mathbf{c}\cdot\nabla h - (\mathbf{v}\cdot\nabla h)' + \left(\frac{\partial h}{\partial t}\right)'_{\text{adi}} + \left(\frac{\partial h}{\partial t}\right)'_{\text{dia}}, \qquad (7)$$

where all the primed terms represent effects observed in a coordinate system moving with the low center. The first term on the right side of (7) may be evaluated by using the known track of the cyclone and the 1000–250 mb thickness analyses shown in I. By integrating over a time interval $\Delta t = t_f - t_i$, we have

$$\int_{t_i}^{t_f}(\mathbf{c}\cdot\nabla h)dt \approx \left(\frac{\overline{\Delta h}}{\Delta s}\right)c(\Delta t) = \overline{\Delta h}, \qquad (8)$$

where $\mathbf{c}\cdot\nabla h = c\Delta h/\Delta s$, and Δs is the length of the Δt displacement vector for speed c. The term $\overline{\Delta h}$ may be written appoximately as

$$\overline{\Delta h} \approx 0.5[(h_{id} - h_{iu}) + (h_{fd} - h_{fu})], \qquad (9)$$

which is the mean of the thickness differences at each time (t_i and t_f) between the observations at the beginning (upstream = u) and end (downstream = d) of the cyclone displacement over time Δt. As an example, h_{id} represents the thickness value at the initial time t_i, and the position of the surface system at the final time.

The effect of temperature advection following the surface center may be approximated by using the observed 900 mb (satellite-derived) and 250 mb winds directly over the center, and assuming the winds to be linearly changing with height and in geostrophic balance. Thus, above the planetary boundary layer, any directional change in the wind with height will imply a change in temperature due to advection. These low-level winds in the vicinity of the low center are shown in Fig. 8, along with the 0000 GMT 10 September 250 mb winds. The upper winds for 1200 GMT on the 9th and 10th are shown in I. The cov-

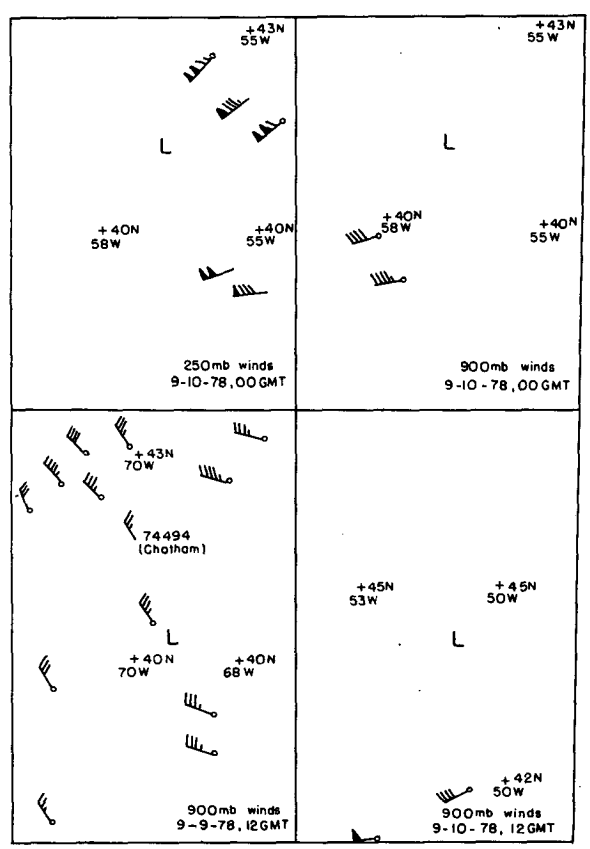

FIG. 8. Wind fields described in text. Winds with open circles are satellite-derived, and those without circles are from commercial aircraft. Position of the surface low is indicated with an "L."

erage is unfortunately sparse near the center at low levels, particularly at 0000 and 1200 GMT on the 10th. Thus, the temperature advection component is likely to be one of the most unreliable in our thickness change budget computations.

Table 1A presents the results of the 24 h budget of thickness change according to expression (7). The numbers in column (1) indicate the observed 12 h thickness changes following the center. The numbers in column (2) represent the thickness change following the center as a result of movement toward higher or lower thickness values,

$$\int_{t_i}^{t_f} (\mathbf{c} \cdot \nabla h) dt = \overline{\Delta h}.$$

The numbers used for this computation are as follows: for the 12 h period beginning 1200 GMT 9 September, h_{id} = 10 320 m, h_{iu} = 10 640 m, h_{fd} = 10 420 m, h_{fu} = 10 580 m; for the 12-h period beginning 0000 GMT 10 September, h_{id} = 10 265 m, h_{iu} = 10 420 m, h_{fd} = 10 725 m, h_{fu} = 10 335 m. These thickness values may be readily identified from the appropriate thickness charts found in I. The column (3) numbers represent the temperature advection effect following the center,

$$\int_{t_i}^{t_f} (\mathbf{v} \cdot \nabla h)' dt.$$

The winds used in this computation are as follows: for the first 6 h period, $\mathbf{v}_{250\,\mathrm{mb}}$ = 314° at 48 m s^{-1}, $\mathbf{v}_{900}$ = 329° at 18 m s^{-1}; for the second and third 6 h periods, $\mathbf{v}_{250}$ = 249° at 55 m s^{-1}, $\mathbf{v}_{900}$ = 255° at 21 m s^{-1} and for the fourth 6 h period, evaluated at a point 200 km south of the center where we have some knowledge of the observed winds $\mathbf{v}_{250}$ = 226° at 28 m s^{-1}, and $\mathbf{v}_{900}$ = 240° at 23 m s^{-1}. The numbers in column (4) are the result of evaluating (6) for moist adiabatic processes. Column (5) numbers indicate the sum of numbers in columns (2) through (4). This sum indicates the predicted thickness change due to large-scale pseudo-adiabatic processes. The resulting predicted thicknesses, due to these processes, are also indicated in column (5) for 0000 and 1200 GMT 10 September. Column (6) shows the residual term, which is accounted for by diabatic processes. We may infer from this table that diabatic processes (excluding latent heating in saturated storm-scale ascent) are required to warm the column 5°C for the first 12 h period, and some 30°C in the second 12 h period. In spite of our relative ignorance of the temperature advection effects discussed earlier and in light of the existing data, it is difficult to imagine enough warm advection to warm the column so dramatically.

To avoid use of the extreme values of vertical motion in computing the 24 h pseudo-adiabatic cooling, we re-estimated term (4) in Table 1B by using a somewhat different technique described by Sanders (1976). The frictionless quasi-geostrophic vorticity equation for sea-level flow may be expressed as

$$\frac{\partial \zeta_{sL}}{\partial t} = -\mathbf{v}_{sL} \cdot \nabla(\zeta_{sL} + f_0) + \eta_0 \left(\frac{\partial \omega}{\partial P}\right)_{sL}, \quad (10)$$

where sL indicates sea-level, f_0 is the Coriolis parameter, and η_0 is the absolute vorticity appropriate to the domain under consideration. The vorticity change at the sea-level cyclone center is due solely to divergence, for advection vanishes here. If we express ζ_{sL} geostrophically as

$$\zeta_{sL} = (\rho_{sL} f_0)^{-1} \nabla^2 P_{sL} \quad (11)$$

and assume a simple two-dimensional harmonic variation of $P_{sL}(x, y)$ with wavelength L and amplitude $\hat{P}_{sL}$, then at the cyclone center, (10) can be expressed as

$$\frac{\partial \hat{P}_{sL}}{\partial t} = -\left(\frac{\rho_{sL} f_0}{2}\right)\left(\frac{L}{2\pi}\right)^2 \eta_0 \left(\frac{\partial \omega}{\partial P}\right)_{sL}. \quad (12)$$

Equation (12) becomes, with the assumption of a linear variation of ω from zero at 1000 mb to a maximum magnitude at 550 mb,

$$\frac{\partial \hat{P}_{sL}}{\partial t} = \left(\frac{\rho_{sL} f_0}{2}\right)\left(\frac{L}{2\pi}\right)^2 \eta_0 \left(\frac{\omega_{550}}{450\ \mathrm{mb}}\right). \quad (13)$$

We approximate (6) by

$$\left(\frac{\partial h}{\partial t}\right)_{\mathrm{adi}} = \left[-\frac{R}{g P_0^{(R/c_P)}}\right]\left(\frac{\omega_{550}}{2}\right) \times \left[\left(\frac{\partial \theta}{\partial P}\right) - \left(\frac{\partial \theta}{\partial P}\right)_{\mathrm{ma}}\right] \int_{250}^{1000} P^{(R/c_P)} d \ln P, \quad (14)$$

where the mean value of ω in this layer is approximated by $\omega_{550}/2$. We will use the temperature stratifications found in Section 2 for each of the times 1200 GMT 9 and 10 September. By eliminating ω_{550} between (13) and (14), and using the equation of state, we have

$$\left(\frac{\partial h}{\partial t}\right)_{\mathrm{adi}} = -T_{sL}(P_{sL} f_0 \eta_0 L^2)^{-1}\left(\frac{\partial \hat{P}_{sL}}{\partial t}\right) \times \left[1.7 \times 10^8\ \mathrm{m^3\ s^{-2}\ K^{-2}\ mb} \times \left(\frac{\partial \theta}{\partial P} - \left(\frac{\partial \theta}{\partial P}\right)_{\mathrm{ma}}\right)\right]. \quad (15)$$

Computations using (15) are summarized in Table 1B. The numbers found for columns (1), (2), and (3) are identical to those found in the earlier computations. We can see less pseudo-adiabatic cooling during the second 12 h period, primarily because we are not using the vertical motion found in the cyclone at the end of its development stage, but rather a more correct integrated value. There is still, however, a 17°C

TABLE 1. Thickness change budget for 24 h period beginning 1200 GMT 9 September 1978.

	Time	Observed 1000–250 mb thickness over center (m)	(1) Observed 12 h thickness change (m)	(2) $\overline{\Delta h}$ (m/12 h)	(3) Temperature advection (m/6 h)	(4) Pseudo-adiabatic cooling (m/12 h)	(5) =(2) + (3) + (4) (m/12 h)	(6) Residual $(\partial h/\partial t)_{dia}$ (1)–(5) (m/12 h)
Part A	1200 GMT 9 September	h = 10 640 m = −10.9°C						
					−48			
			−220	−240		−117	−432	+212
[column 4 using Eq. (6)]					−27			
	0000 GMT 10 September	h = 10 420 m = −16.3°C					predicted h = 10 208 m = −21.6°C	
					−27			
			+305	+118		−942	−885	+1190
					−34			
	1200 GMT 10 September	h = 10 725 m = −8.8°C					predicted h = 9535 m = −38.2°C	
Part B	1200 GMT 9 September	column (4) parameters for Eq. (15) T_{sL} = 288 K P_{sL} = 1000 mb $f_0 = 9.4 \times 10^{-5}$ s^{-1} $\eta_0 = 2.0 \times 10^{-4}$ s^{-1}	$L = 1.5 \times 10^6$ m $(\Delta P/\Delta t)$ = −14 mb/12 h			from Eq. (15): −152	−467	+247
[column 4 using Eq. (15)]	0000 GMT 10 September						predicted h = 10 173 m = −22.4°C	
	1200 GMT 10 September	column (4) parameters for Eq. (15) T_{sL} = 288 K P_{sL} = 970 mb $f_0 = 9.8 \times 10^{-5}$ s^{-1} $\eta_0 = 3.0 \times 10^{-4}$ s^{-1}	$L = 1.8 \times 10^6$ m $(\Delta P/\Delta t)$ = −45 mb/12 h			−417	−360	+665
							predicted h = 10 060 m = −25.2°C	

mean temperature increase in the column evidently affected by non-pseudo-adiabatic processes. Possible processes responsible for this warming will now be discussed.

Surface sensible heating following the low center is a negligible quantity, since the horizontal wind speed at the cyclone center is negligible. This is consistent with findings of Petterssen *et al.* (1962) which indicate strong sensible heating is confined to the southwest of the storm center in the heart of the cold-air outbreak. Any sensible heating would be largest near the surface and thus tend to destroy potential vorticity slightly, through static destabilization.

The radiative effects, such as long-wave cooling at cloud tops are O(2–3 K/12 h) and in the 1000–250 mb column, may account for as much as a 1 K temperature decrease (Manabe, 1956), or a 40 m tropospheric thickness decrease. Resulting storm-scale potential vorticity changes will be small, for the layers in which substantial heating gradients exist are quite thin.

The diabatic effect we have yet to consider is the cumulus-induced subsidence warming. Evidence for this is found in the clear eye-like area in the storm center. Smith (1980) has estimated the magnitude of this descent in the eye of a tropical cyclone to be about 10 cm s^{-1}. A parabolic profile of this subsidence with the observed temperature structure will yield a column warming of 16°C in 12 h. This number is sufficient to balance the thickness change budget of Table 1. The resulting potential vorticity increase below the peak in the subsidence warming profile due to the stability change term in (4a) is O[10^{-5} s^{-1} K mb^{-1} (12 h)$^{-1}$], which is one order of magnitude less than the observed potential vorticity increase found over the center. However, mesoscale horizontal (~500 km distance) variations [see tilting term in (4a)] of this subsidence effect yield a potential vorticity increase approaching the observed. Therefore, it appears that the compensating subsidence, apparently important in accounting for the strong warming over the storm center, is concurrently important in enhancing potential vorticity. Although strong cyclone-scale ascent has been computed for this case, the satellite images, shown in I, indicate deep convective elements with adjacent cloudless areas within this region of strong storm-scale ascent. This fact is critical for the modification of the thermodynamic and dynamic structure of this cyclone. The next section examines the dynamical consequences of these cumulus-induced heating effects.

5. The dynamical effects of heating on the cyclogenesis

The preceding analysis has indicated a 25–35°C mean tropospheric warming over the surface low center during its 24 h explosive development subsequent to 1200 GMT 9 September. The primary cause of this warming appeared to be due to bulk heating effects of the cumulus convection observed during this period. The purpose of this section is to quantify the dynamical effects such heating might have on the development of the cyclone itself.

Much attention has been paid in the literature to the ensemble effects of cumulus convection on the dynamics of the tropical cyclone. In particular, numerical modelers such as Yamasaki (1968) and Ooyama (1969) have indicated a strong sensitivity of a vortex to how these heating effects are distributed vertically. Koss (1976), in a linear stability analysis of CISK-induced disturbances, also found that properties of cyclone-scale disturbances are dependent upon the vertical heating distribution.

The effect of varying this vertical heating distribution on extra-tropical cyclone development was also found by Anthes and Keyser (1979) to be important. Tracton (1973) estimated the size and magnitude of the bulk cumulus latent heating effects upon continental United States cyclones, with an assumed two-dimensional heating distribution in the lower and upper troposphere. Quasi-geostrophic computations of the 1000 mb geopotential tendency were made for various ratios of upper-to-lower tropospheric heating. The strong sensitivity of computed 1000 mb geopotential falls to this ratio was demonstrated.

We will quantify the dynamical effects of cyclone-scale heating in a more general form than Tracton's analysis allowed, for a three-dimensional distribution of the heating will be specified analytically, allowing for analytic solutions to both the quasi-geostrophic ω and vorticity equations.

The quasi-geostrophic ω-equation forced by diabatic temperature changes (Danard, 1964) may be expressed as

$$\left(\nabla^2 + \frac{f_0\eta_0}{\sigma}\frac{\partial^2}{\partial P^2}\right)\omega = -\frac{R}{\sigma P c_p}\nabla^2\dot{Q}, \qquad (16)$$

where σ is a function of pressure only, and is defined (see Sanders, 1971) as $\sigma(P) = RT_0\gamma P^{-2}$, where T_0 is the mean tropospheric temperature, $\dot{Q}$ the diabatic heating per unit mass, c_p the specific heat of air at constant pressure and γ and the rest of the symbols are defined in the Appendix of I.

A key question to be asked is the validity of the quasi-geostrophic approximation, considering such a rapid cyclogenesis occurred. Since (16) only involves heating, the approximations with regard to vorticity advection effects are not considered here. The approximation neglecting the relative vorticity ζ compared with f in the divergence term of the vorticity equation will be relaxed, and the implications of this will be discussed. The approximation of the vorticity by its geostrophic value is a weakness of this

procedure, which will cause us to underestimate the computed height falls. Thus, we may use this system of equations with the knowledge that our pressure fall computations will be conservative estimates.

We specify this heating function to be zero at the 1000 mb surface and at the top of the atmosphere, with a peak at some intermediate pressure surface P_I. The horizontal distribution will be given by a two-dimensional harmonic variation so that in layer 1:

$$\dot{Q} = \frac{(P_0 - P)2Bg}{(P_0 - P_I)P_0} \cos\left(\frac{2\pi x}{L}\right) \cos\left(\frac{2\pi y}{M}\right), \quad P_I \leq P \leq P_0, \tag{17a}$$

and in layer 2:

$$\dot{Q} = \frac{P(2Bg)}{P_I P_0} \cos\left(\frac{2\pi x}{L}\right) \cos\left(\frac{2\pi y}{M}\right), \quad 0 \leq P \leq P_I, \tag{17b}$$

where B represents the total heating in the column $[g^{-1} \int_0^{P_0} \dot{Q}(P)dP]$, P_0 is the reference pressure (1000 mb), and L and M are the wavelengths of the heating perturbation in the x and y-directions, respectively.

A representation of the heating function's vertical variation is given in Fig. 9. The arbitrary specification of the peak in heating at a particular pressure level P_I is a simple means by which we may assess the dynamical importance of the vertical distribution of heating. Although our idealized heating profile extends unrealistically up to the top of the atmosphere, this problem above the tropopause will not seriously affect the tropospheric ω-profiles, and the resulting geopotential tendencies for a surface disturbance. The vertically-integrated heating range previously described (12–17°C 12 h^{-1}) corresponds approximately to a 1000–250 mb thickness rise of from 500–700 m/12 h. If all of this heating were realized as condensation, rainfall rates of from 0.32 to 0.45 cm h^{-1} would be found. Although this implied heating is about five times that of Phillips' (1963) theoretical limit of 0.08 cm h^{-1} for the quasi-geostrophic approximation to be strictly valid, this small discrepancy should not alter the basic results of these calculations. Moreover, our values are still considerably less than the 3 cm h^{-1} value often observed raining out of individual convective cells.

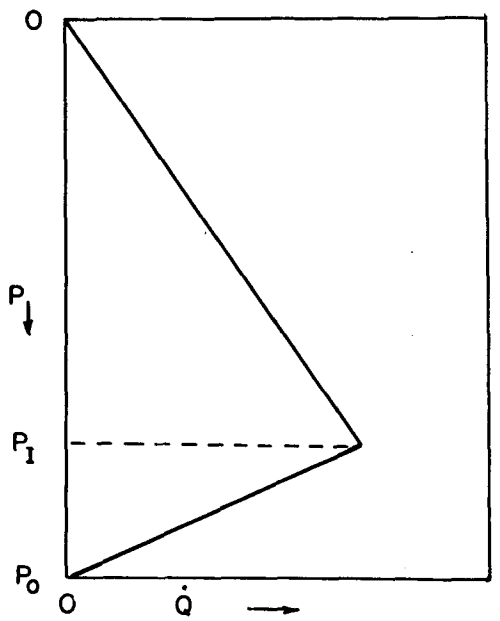

FIG. 9. Vertical profile of the heating function described in the text.

The prescribed heating functions specify an ω-equation in each layer, so that in layer 1:

$$\left(\nabla^2 + \frac{f_0\eta_0}{\sigma}\frac{\partial^2}{\partial P^2}\right)\omega = \frac{b_1(P_0P - P^2)2Bg}{(P_0 - P_I)P_0T_0\gamma c_p} \times \cos\left(\frac{2\pi x}{L}\right)\cos\left(\frac{2\pi y}{M}\right), \quad P_I \leq P \leq P_0, \tag{18a}$$

in layer 2:

$$\left(\nabla^2 + \frac{f_0\eta_0}{\sigma}\frac{\partial^2}{\partial P^2}\right)\omega = \frac{b_1P^2 2Bg}{P_IP_0T_0\gamma c_p} \times \cos\left(\frac{2\pi x}{L}\right)\cos\left(\frac{2\pi y}{M}\right), \quad 0 \leq P \leq P_I, \tag{18b}$$

where $b_1 = (2\pi/L)^2 + (2\pi/M)^2$. Solving the second-order differential equations (18a) and (18b) involves specifying the boundary conditions; the first shall be $\omega = 0$ at the lower boundary of layer 1 (at $P = P_0$), and the second to be $\omega = 0$ at $P = 0$. The other two boundary conditions are at the interface between the two layers: i.e., ω and $\partial\omega/\partial P$ match at $P = P_I$.

The solution for ω forced by our heating function $\dot{Q}$, is, for the first layer:

$$\omega_H = C_H P^{q_1} + D_H P^{q_2} - \frac{k_{H1}P}{b_1} - \frac{k_{H2}P^2}{(2a_1 - b_1)}, \quad P_I \leq P \leq P_0, \tag{19a}$$

and in the second layer:

$$\omega_H = A_H P^{q_1} + \frac{k_{H3}P^2}{(2a_1 - b_1)}, \quad 0 \leq P \leq P_I, \tag{19b}$$

where

$$k_{H1} = \frac{(b_1P_0)(2Bg)}{(P_0 - P_I)(P_0T_0\gamma c_p)} \cos\left(\frac{2\pi x}{L}\right)\cos\left(\frac{2\pi y}{M}\right),$$

$$k_{H2} = \frac{k_{H1}}{P_0},$$

$$k_{H3} = \frac{b_1(2Bg)}{(P_IP_0T_0\gamma c_p)} \cos\left(\frac{2\pi x}{L}\right)\cos\left(\frac{2\pi y}{M}\right),$$

$$A_H = \frac{k_{H1}P_0^{(1-q_1)}}{b_1} + \frac{k_{H2}P_0^{(2-q_1)}}{(2a_1 - b_1)} - \frac{(q_2 - 1)k_{H1}P_I^{q_2}}{b_1(q_2 - q_1)}$$
$$- \frac{(q_2 - 2)(k_{H2} + k_{H3})P_I^{(q_2+1)}}{(2a_1 - b_1)(q_2 - q_1)} + \frac{P_0^{(q_2-q_1)}(q_1 - 1)k_{H1}P_I^{q_1}}{b_1(q_2 - q_1)}$$
$$+ \frac{P_0^{(q_2-q_1)}(q_1 - 2)(k_{H2} + k_{H3})P_I^{(q_1+1)}}{(2a_1 - b_1)(q_2 - q_1)},$$

$$C_H = \frac{k_{H1}P_0^{(1-q_1)}}{b_1} + \frac{k_{H2}P_0^{(2-q_1)}}{(2a_1 - b_1)} + \frac{P_0^{(q_2-q_1)}(q_1 - 1)k_{H1}P_I^{q_1}}{b_1(q_2 - q_1)}$$
$$+ \frac{P_0^{(q_2-q_1)}(q_1 - 2)(k_{H2} + k_{H3})P_I^{(q_1+1)}}{(2a_1 - b_1)(q_2 - q_1)},$$

$$D_H = \frac{(1 - q_1)k_{H1}P_I^{q_1}}{b_1(q_2 - q_1)} + \frac{(2 - q_1)(k_{H2} + k_{H3})P_I^{(q_1+1)}}{(2a_1 - b_1)(q_2 - q_1)},$$

where $a_1 = f_0\eta_0/(RT_0\gamma)$, $q_1 = 0.5 + 0.5(1 + 4(b_1/a_1))^{1/2}$ and $q_2 = 1 - q_1$.

The geopotential height falls at 1000 mb associated with these heating-induced vertical motions may be found by expressing the quasi-geostrophic vorticity equation as

$$\nabla^2(\partial\Phi/\partial t) = f_0\eta_0\left(\frac{\partial\omega}{\partial P}\right), \tag{20}$$

where the vorticity is expressed geostrophically as $\zeta = \nabla^2\Phi/f_0$. $\partial\omega/\partial P$ is obtained at 1000 mb by differentiating the solution (19a) and evaluating it at $P = P_0 = 1000$ mb. Assuming that $\partial\Phi/\partial t$ has the same horizontal structure as the corresponding forcing function $f_0\eta_0(\partial\omega/\partial P)$, (20) may be expressed as

$$\chi = \partial\Phi/\partial t = -\left(\frac{f_0\eta_0}{b_1}\right)\frac{\partial\omega}{\partial P}, \tag{21}$$

so that the geopotential height tendency χ_H is

$$\chi_H = \hat{\chi}_H(1000\text{ mb})\cos\left(\frac{2\pi x}{L}\right)\cos\left(\frac{2\pi y}{M}\right)$$

and

$$\hat{\chi}_H = -\frac{f_0\eta_0}{b_1}\left\{\frac{\left[\left(\frac{P_I}{P_0}\right)^{q_1} - 1\right]k_{H1}(1 - q_1)}{b_1}\right.$$
$$\left. + \frac{\left[(k_{H2} + k_{H3})P_I\left(\frac{P_I}{P_0}\right)^{q_1} - k_{H2}P_0\right](2 - q_1)}{(2a_1 - b_1)}\right\}. \tag{22}$$

Expression (22) indicates that, from the definitions of K_{H1}, K_{H2}, and K_{H3}, $\hat{\chi}_H$ is linearly proportional to B (the vertical integral of the heating defined after 17b), and also depends upon P_I (the pressure level of the heating maximum), the vorticity–stability parameter $f_0\eta_0(T_0\gamma)^{-1}$, and the wavelengths L and M. The calculations in this section will assume $f_0 = 1.0 \times 10^{-4}$ s^{-1} (the Coriolis parameter at 45° latitude), $T_0 = 250$ K, and $L = M$.

Fig. 10 shows $\hat{\chi}_H$ as a function of wavelength and P_I, for two vorticity-stability values. For a typical

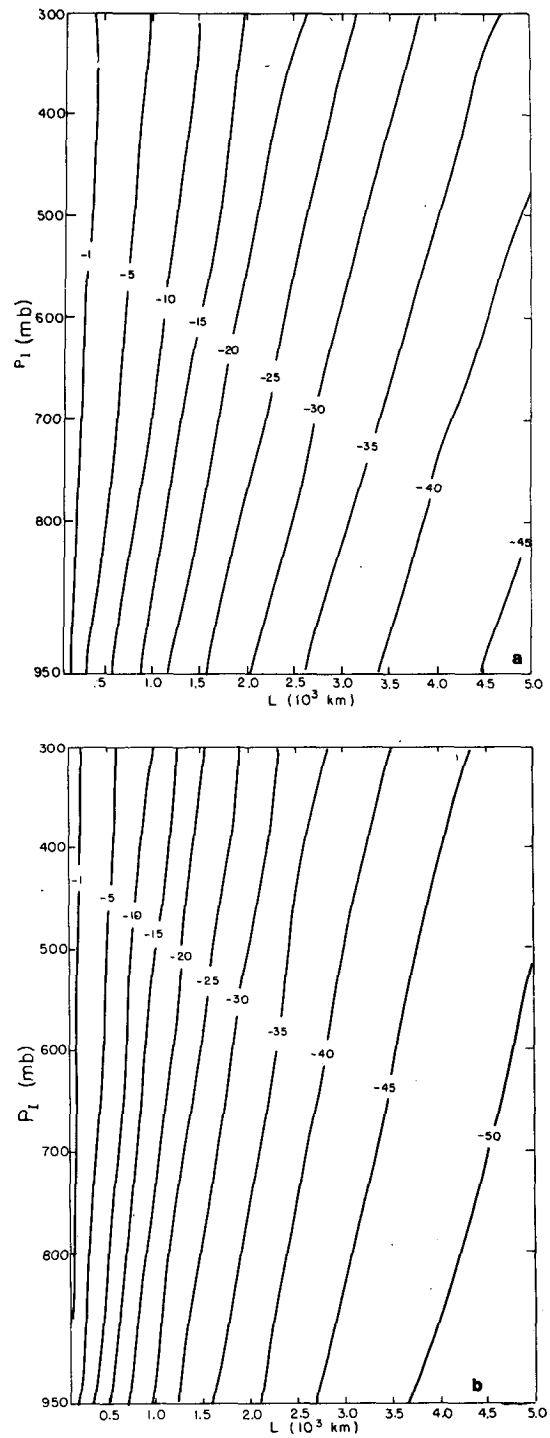

FIG. 10. Values of geopotential tendency $\hat{\chi}_H$ (10^{-3} m^2 s^{-3}) as a function of wavelength and peak level of heating P_I. Values of vorticity–stability include (a) 1.0×10^{-9} and (b) 2.7×10^{-9} s^{-2} K^{-1}.

static stability value γ of 0.06, these values would correspond to absolute vorticity (η_0) values of 1.5 and 4.0 $\times$ 10^{-4} s^{-1}. All of these calculations are for $B = 21.9$ (m s^{-1}) mb, corresponding to a 12 h heating-induced 1000–250 mb thickness increase of 500 m for a mean column warming of 12.3°C 12 h^{-1}. This is the lower-bound heating value computed over the surface cyclone center during its 24 h explosive development period. Greater height falls are noted as P_1 increases, and also, as the wavelength increases.

A fundamental question to ask is, what process(es) can organize these bulk heating effects? Clearly, the cyclone-scale is not seen as the preferred wavelength for deepening in Fig. 10. It appears plausible, from the analyses of the composite explosive cyclone in Sanders and Gyakum (1980, hereafter referred to as SG) and this case, that baroclinic forcing, though quite weak itself, organizes the convective towers such that their bulk heating effects have a scale comparable to the cyclone itself. A concurrent discussion of quasi-geostrophic baroclinic development and cumulus convection may appear to be inconsistent. Indeed, if the environment is gravitationally unstable on the cyclone-scale, the assumptions under which the quasi-geostrophic system of equations are derived become invalid. However, SG and our observations of this case indicate that large-scale static instability does not appear to be a regular feature of the explosively-developing extratropical cyclone. Yet, cumulus convection does appear as a regular feature in this and other cases. Thus, we are arguing in favor of an environment that is statically stable for cyclone-scale motions, yet is gravitationally unstable for the micro- or cumulus-scale. Indeed, the satellite images in I, and the large-scale *conditionally* unstable environment in which it developed (see Fig. 5b), comparable images of the extraordinary cyclogenetic event on President's Day, 1979 (Bosart, 1981), and Tracton's (1973) cases, all show a cyclone-scale environment that is unsaturated, yet associated with cumulus activity. This is precisely the basis for the CISK argument set forth by Charney and Eliassen (1964) in their study of the hurricane development problem. We now know from SG that the bomb has comparably-strong deepening rates to some of the most explosively-developing tropical cyclones. We now test this CISK-like hypothesis, as applied to this case.

Fig. 11 shows the geopotential tendency $\hat{\chi}_{10}$ (for $\hat{T} = 1$°C) from the pseudo-adiabatic quasi-geostrophic model described in I. With all other parameters fixed, the geopotential tendency is linearly proportional to $\hat{T}$ (the perturbed part of the temperature field as defined by Sanders, 1971). P_2 and P_3 are chosen to be 800 and 400 mb, respectively, to correspond to the computations performed for this case at 1200 GMT 9 September. Fig. 11 also shows qualitative similarity to the results of Sanders, namely that the deepening or instability of the baroclinic system is enhanced with increasing values of unperturbed temperature gradient and vorticity-stability parameter. The wavelength of maximum instability, however, is found at the relatively short wavelengths of between

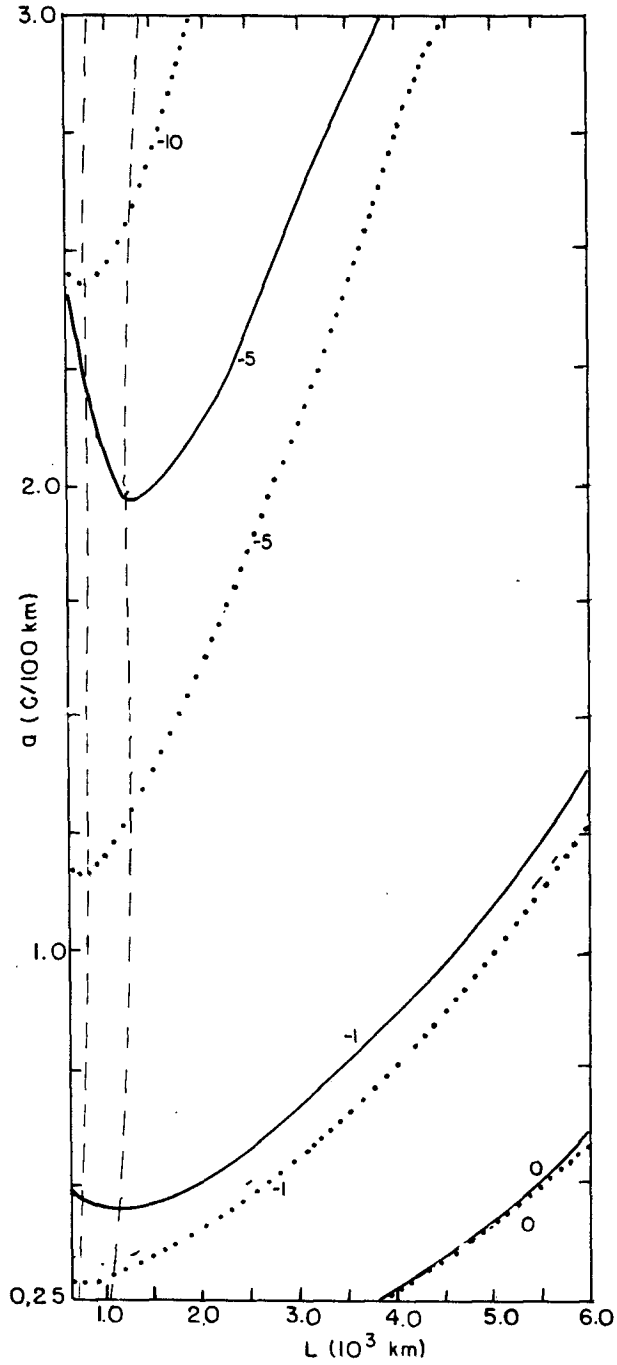

FIG. 11. Geopotential tendency $\hat{\chi}_{10}$ (units of 10^{-3} m^2 s^{-3}) as a function of wavelength L and meridional temperature gradient a for $\hat{T} = 1$°C. Vorticity–stability values as in Fig. 10, and are indicated in their ascending magnitudes by solid and dotted lines. Light dashed lines indicate the loci of the wavelength of maximum deepening rate.

900 and 1200 km; for we are modeling a shallow baroclinic disturbance. These relatively short preferred wavelengths are consistent with Staley and Gall's (1977) finding for disturbances forced by a shallow layer of baroclinicity. We found in I that, even though the observed scale of temperature perturbation in the *QE II* case matched the wavelength of maximum baroclinic instability described in our model, this pseudo-adiabatic baroclinic forcing vastly underestimates both ascent and the instantaneous intensification of the surface cyclone. However, the key aspect of this physical process, is its capacity to organize the heating modeled by (17) on a scale comparable to the cyclone itself. This leads us to choose the parameters necessary for computing the diabatically-forced geopotential fall χ_H.

We have computed vertical motions forced by our model heating distribution using the lower-bound value of integrated heating (24°C/24 h) and the parameters used in I for 1200 GMT 9 September. The heating pattern is assumed to be organized on a scale comparable to the cyclone, so that $L = M = 1100$ km, $\eta_0 = 1.3 \times 10^{-4}$ s^{-1}, and $\gamma = 0.058$. Fig. 12a shows the vertical motion profiles according to expressions (19a) and (19b) for various values of P_I. We can see that, in spite of the same amount of heating in the column (corresponding to a rainfall rate of 0.32 cm h^{-1}, if all of this heating is the result of condensation), the manner in which this heating is distributed vertically has a large effect on the vertical motion profiles it forces. Clearly, the lower the heating maximum, the lower the level of maximum ascent, therefore, the stronger the convergence will be at 1000 mb. The resulting instantaneous central pressure falls, computed from (22), have been linearly extrapolated out to 24 h and are also shown in Fig. 12b as dashed lines. The dotted line indicates the observed central pressure of the cyclone at 1200 GMT 10 September. Consistent with the results of Fig. 10, and our ascent profiles, the choice of P_I has a large effect on central pressure falls, with our numbers ranging from −18.8 mb/24 h for $P_I = 900$ mb to −6.3 mb/24 h for $P_I = 300$ mb.

The linear extrapolation of the instantaneous value of $\eta_0(\partial\omega/\partial P)$ for such long time periods as 24 h is inaccurate, for the time rate of change of relative vorticity is itself a function of the relative vorticity. Thus, if we now express (20) as

$$\frac{\partial \ln\eta}{\partial t} = \frac{\partial \omega}{\partial P}. \tag{23}$$

Here η will grow exponentially with time for a constant $(\partial\omega/\partial P)$. We can then compute the geopotential falls by expressing the vorticity geostrophically as we did earlier in this section. Thus,

$$\eta_{\text{geostrophic}}(t) = \eta_{\text{geostrophic initial}} \exp\left[\left(\frac{\partial \omega}{\partial P}\right)t\right]. \tag{24}$$

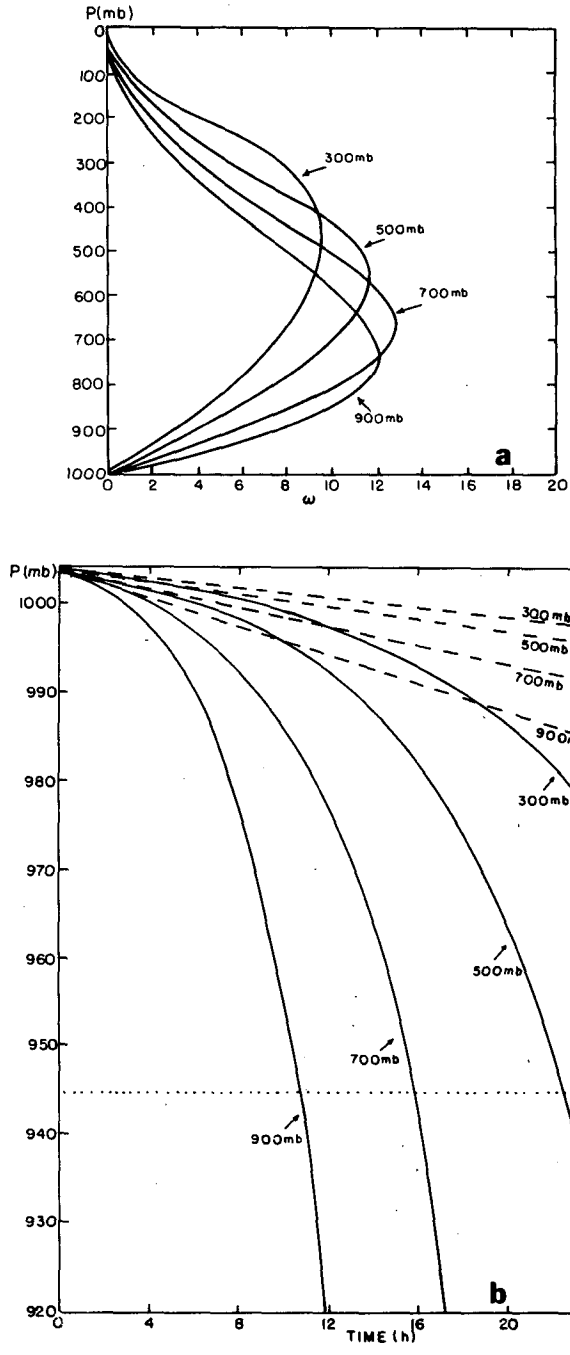

FIG. 12. (a) Heating induced vertical motion (10^{-3} mb s^{-1}) profiles at 1200 GMT 9 September 1978 for the indicated values of P_I and for $B = 21.9$ m s^{-1} mb. (b) Theoretical linear and nonlinear pressure traces as a function of time, and beginning at 1200 GMT 9 September for the same parameters as in (a) and for the indicated P_I values. Dotted line shows the central pressure of the storm at the end of the 24 h period (1200 GMT 10 September).

Although this procedure is a vast improvement over our previous assumption of a constant value of $\eta_0(\partial\omega/\partial P)$ with time, there are still two reasons why our method will underestimate the actual central

pressure fall due to this inviscid forcing. The first is that $(\partial\omega/\partial P)$ itself is a function of time, and generally increases with time in an intensifying cyclone. Next, as noted earlier, the winds are more likely to be in gradient, rather than in geostrophic balance. Thus, for a given amount of divergence, a greater height fall would be diagnosed under gradient balance conditions, than would be shown with the assumption of geostrophic balance. This is the key weakness of the quasi-geostrophic approximation, so we know *a priori* our pressure fall calculations will be conservative.

Fig. 12b shows the central pressure changing with time (solid lines) according to (24). It appears the exponential heating-forced deepening rates easily account for the observed 24 h intensification, for choices of P_I below the 500 mb level.

Computations using the upper-bound estimate of heating forcing a 1400 m/24 h warming of the column have been performed with the other parameters fixed. The vertical motions are exactly 1.4 times those found in Fig. 12 for a given P_I and P. The linear central pressure falls are also increased by a factor of 1.4, but the pressure traces using (24) are changed, so that with P_I's below the 300 mb level, they more than account for the observed 24 h central pressure fall. The retention of ζ in the divergence term of (23) is a relaxation of the quasi-geostrophic approximation which allows us to compute these relatively large pressure falls. Of course, these calculations do not take into account surface frictional dissipation, so we should expect a larger central pressure fall than observed. If, indeed, the heating is distributed horizontally so as to reach a maximum at the surface low center, or at least the Laplacian of the heating is negative at the surface center, our calculations imply a positive feedback between the cyclone and convective scales, not unlike a CISK process. Here, shallow baroclinic instability apparently helps to organize the convection in such a way as to effect the bulk heating distribution, which in turn, provides a powerful dynamic intensification mechanism for the cyclone scale. This cyclone-scale intensification helps to converge more moisture into its center, thus helping the convection to maintain itself. Thus, even with the relatively weak baroclinic forcing found for this case, when it is combined with various hypothesized three-dimensional heating distributions, our quasi-geostrophic calculations show explosive development for virtually all sets of reasonable heating profiles.

We also performed an independent check on consistency between our quasi-geostrophic surface convergences, with the implicit vertical motions used for the adiabatic cooling computations in column (4) of Table 1B. The 24 h time-mean surface convergence implied by expression (15) for these thickness-change computations is 7×10^{-5} s^{-1}. Note this implicit vertical motion would include both the diabatically-forced and baroclinic components of ω, although there is no representation of the component of ascent due to surface frictional convergence. Thus, it would be satisfying to know that this implied "observed" convergence would be comparable to the sum of our theoretical baroclinic and diabatic surface convergences. The 1000 mb convergence implied by the baroclinic computations from Table 2 of I is 2.9×10^{-5} s^{-1} and the 1000 mb convergences implied by the heating computations range from 2.9×10^{-5} s^{-1} [for P_I = 300 mb and B = 21.9 (m s^{-1}) mb] to 12×10^{-5} s^{-1} [for P_I = 900 mb, and B = 30.7 (m s^{-1}) mb]. Thus, while the component of vertical motion due to baroclinic forcing alone is insufficient to account for the observed divergence, the addition of the diabatically-forced surface convergence will allow the sum of these two convergences to account for the implicit "observed" convergence.

Thus, our observations of the explosive intensification of the *QE II* storm, concurrent with the development of its strong warm core, are all consistent with our quasi-geostrophic calculations, which incorporate both diabatic and baroclinic forcing. While adiabatic, inviscid, quasi-geostrophic dynamics are unable to explain the observed explosive intensification, the total amount of heating observed for the column can be modeled quasi-geostrophically, and will simulate the observed rapid cyclogenesis found in this case, throughout the spectrum of uncertainty of our measurements.

The foregoing statements lead us to question why the operational numerical models simulated this storm so poorly. Possible reasons include poor initial data, inadequate vertical and horizontal computational resolution, and improper simulation of such physical processes as the bulk effects of cumulus convection. The available evidence hints strongly that, since the cumulus-induced heating appeared to be of first-order importance in this case, the operational models may have failed to properly simulate the cumulus effects. This hypothesis is consistent with the conclusions of Tracton, among others.

Our results have potentially important implications for numerical modelers. If these bulk cumulus effects are as important for other cases of rapid maritime cyclogenesis, then a closer examination of existing cumulus schemes needs to be undertaken. Work is continuing on possible reasons for the numerical model's poor performance, and this will be reported upon in a companion paper.

6. Conclusions

The convection associated with the explosively-developing cyclone of September 1978 as shown in part I of this study has provided us with a motivation to assess the importance of heating on this cyclone's development. To accomplish this, we have devised as method of evaluating the three-dimensional ther-

modynamic and dynamic structure of the atmosphere in order to evaluate potential vorticity changes in the vicinity of the storm. Results indicate a 24 h lower tropospheric generation of from five to thirteen times the values observed at the initial time. Our calculations have shown a large mean tropospheric temperature rise in the column following the storm center to be due to bulk heating effects of the observed cumulus convection. It is probable that these bulk heating effects of the observed (in I) convective towers in this case (through the horizontal Laplacian of diabatic temperature change) drove much of the storm-scale ascent not accounted for by our pseudo-adiabatic, inviscid quasi-geostrophic calculations. These effects likely caused the large potential vorticity increase in the cyclone, along with the concurrent intensification not accounted for by the operational numerical model forecasts. Thus, we do not need to invoke the "cumulus friction" effect to explain the large potential vorticity increase. The most likely bulk heating effect responsible for the warm core, explosive cyclogenesis, and potential vorticity generation appears to be the cumulus-induced compensating subsidence.

We have utilized these observed vertically-integrated values of heating as a motivation for finding analytic solutions to the quasi-geostrophic omega equation forced by an idealized heating function, with specified horizontal scale, level of maximum heating P_I and total heating. The theoretical geopotential height falls calculated from the quasi-geostrophic vorticity equation over a 24 h period for the observed vertically-integrated values of heating, vorticity–stability, and over a wide range of horizontal scales and levels of heating peaks easily account for the large observed pressure falls. A particularly large sensitivity of growth rate to P_I was noted. This provides theoretical support for the numerical results of Yamasaki (1968), Ooyama (1969), and Anthes and Keyser (1979), all of whom found such a sensitivity in their simulations of both extratropical and tropical disturbances associated with cumulus convection.

The largest growth rates due to this heating function are found for the lowest levels of heating maximum. The reason for this is obvious, for the level of maximum forced ascent is lowered under these conditions, thereby producing a larger value of surface convergence. Evidence exists that relatively low levels of heating did, in fact, occur in this case. In spite of a strong tropospheric warm core observed in the disturbance (Fig. 12 in I), a comparably large temperature perturbation is not observed at 250 mb (Fig. 1b), and aircraft temperatures recorded in the mid-troposphere indicate the soundings over the center with the lowest-level warm temperature perturbations to be the most realistic (Fig. 3b). More cases need to be documented in a manner similar to that performed for this case to verify the generality of such conclusions.

We have established both observationally and theoretically the critical importance cumulus-induced heating effects may have in determining whether a cyclone explosively intensifies or not. Although the CISK mechanism is a plausible means by which explosive cyclogenesis is accomplished in both hurricanes and "bombs," key questions about how the organization of the cumulus is effected, as well as important aspects of its interaction with the larger-scale features, remain.

Baroclinic instability appears to be directly responsible for a small part of this case's development, but more importantly it organized the convective effects in such a way as to produce a positive feedback and the explosive development. Other cases may also be baroclinically unstable and contain convection, but because of differences in the dynamic and thermodynamic atmospheric structure which could dictate an unfavorable feedback between the two processes, explosive development may be absent.

The successful prediction of the cumulus convection effects, as described in this paper, appear lacking. Accurate precipitation forecasts generated by existing cumulus parameterizations, (Krishnamurti *et al.*, 1980) are not sufficient. Rather, a performance evaluation of the various cumulus schemes in predicting the vertical distributions of thermodynamic changes due to the cumulus, particularly in the extratropics, seems necessary. Unfortunately, Lord (1982) has found this simulation to be a deficiency of the Arakawa and Schubert (1974) parameterization in spite of success being reported with predicting the vertically-averaged cumulus effects.

In fact, the issue of whether the cumulus effects on the larger scale can be expressed in terms of the larger-scale variables should be re-examined. If this is not the case, then cumulus parameterization is not possible, for implicit in all cumulus schemes is the assumption of a time-scale separation between the large-scale and cloud-scale processes. This separation is not as clear when one considers that MCC's (Maddox, 1980) are often associated with tropical cyclones (Weickmann *et al.*, 1977), flash floods and explosive cyclogenesis (Bosart and Sanders, 1981). These latter features, in turn, may influence the larger-scale general circulation. This scale interaction, along with the one described in this paper, provide us with more motivation to examine further the mutual interaction between cloud, meso-, and synoptic scale motions.

Acknowledgments. This study represents a portion of the author's Ph.D. dissertation at the Massachusetts Institute of Technology. The author is especially grateful to his advisor, Professor Frederick Sanders, whose direction and comments have helped considerably to improve upon this work. I thank Professors Mark Cane and Lance Bosart for making many helpful comments and engaging in many stimulating dis-

cussions about maritime cyclogenesis. Professor Cane, along with Dr. Vince Cardone of Oceanweather, Inc., provided the Seasat data set. Members of the MIT convection club and fellow students, including Dr. George Huffman, Dr. Frank Colby, Brad Colman, Dr. Randy Dole, and Dr. Frank Marks made many helpful comments. Dr. Steve Tracton of the National Meteorological Center helped me to obtain the *Euroliner* log and barogram from the British Meteorological Office. Special thanks go to Dr. Alan Weinstein, Director of Research at the Naval Environmental Prediction Research Facility (NEPRF), for his genuine interest in this work. Ms. Isabelle Kole did a superb job in drafting the figures, while Karen Garrelts and Norene McGhiey typed the manuscript. This research was supported by the Office of Naval Research, and by NEPRF under Contract N00014-79-C-0384.

REFERENCES

Anthes, R. A., and D. Keyser, 1979: Tests of a fine-mesh model over Europe and the United States. *Mon. Wea. Rev.*, **107**, 963–984.

Arakawa, A., and W. H. Schubert, 1974: Interaction of a cumulus cloud ensemble with the large-scale environment. Part I. *J. Atmos. Sci.*, **31**, 674–701.

Bosart, L. F., 1981: The President's Day snowstorm of 18–19 February 1979: A subsynoptic scale event. *Mon. Wea. Rev.*, **109**, 1542–1566.

——, and F. Sanders, 1981: The Johnstown flood of July 1977: A long-lived convective storm. *J. Atmos. Sci.*, **38**, 1616–1642.

Charney, J. G., and A. Eliassen, 1964: On the growth of the hurricane depression. *J. Atmos. Sci.*, **21**, 68–75.

Danard, M. B., 1964: On the influence of released latent heat on cyclone development. *J. Appl. Meteor.*, **3**, 27–37.

Ertel, H., 1942: Ein neuer hydrodynamischer wirbelsatz. *Meteor. Z.*, **59**, 277–281.

Gidel, L. T., and M. A. Shapiro, 1979: The role of clear air turbulence in the production of potential vorticity in the vicinity of upper tropospheric jet streams–frontal systems. *J. Atmos. Sci.*, **36**, 2125–2138.

Gyakum, J. R., 1983: On the evolution of the *QE II* storm. I: Synoptic aspects. *Mon. Wea. Rev.*, **111**, 1137–1155.

Harrold, T. W., and K. A. Browning, 1969: The polar low as a baroclinic disturbance. *Quart. J. Roy. Meteor. Soc.*, **95**, 710–723.

Holton, J. R., 1972: *An Introduction to Dynamic Meteorology.* Academic Press, 320 pp.

Koss, W. J., 1976: Linear stability of CISK-induced disturbances: Fourier component eigenvalue analysis. *J. Atmos. Sci.*, **33**, 1195–1222.

Krishnamurti, T. M., Y. Ramanathan, H.-L. Pan, R. J. Pasch and J. Molinari, 1980: Cumulus parameterization and rainfall rates I. *Mon. Wea. Rev.*, **108**, 465–472.

Lord, S. J., 1982: Interaction of a cumulus cloud ensemble with the large-scale environment. Part III: Semi-prognostic test of the Arakawa–Schubert cumulus parameterization. *J. Atmos. Sci.*, **39**, 88–103.

Maddox, R. A., 1980: Mesoscale convective complexes. *Bull. Amer. Meteor. Soc.*, **61**, 1374–1387.

Manabe, S., 1956: On the contribution of heat released by condensation to the change in pressure pattern. *J. Meteor. Soc. Japan*, **34**, 308–320.

Mansfield, D. A., 1974: Polar lows: The development of baroclinic disturbances in cold air outbreaks. *Quart. J. Roy. Meteor. Soc.*, **100**, 541–554.

Ooyama, K., 1969: Numerical simulation of the life cycle of tropical cyclones. *J. Atmos. Sci.*, **26**, 3–40.

Petterssen, S., D. L. Bradbury and K. Pedersen, 1962: The Norwegian cyclone models in relation to heat and cold sources. *Geofys. Publ.*, **24**, 243–280.

Phillips, N. A., 1963: Geostrophic motion. *Rev. Geophys.*, **1**, 123–176.

Rasmussen, E., 1979: The polar low as an extratropical CISK disturbance. *Quart. J. Roy. Meteor. Soc.*, **105**, 531–549.

Reed, R. J., 1979: Cyclogenesis in polar air streams. *Mon. Wea. Rev.*, **107**, 38–52.

Sanders, F., 1971: Analytic solutions of the nonlinear omega and vorticity equations for a structurally simple model of disturbances in the baroclinic westerlies. *Mon. Wea. Rev.*, **99**, 393–407.

——, 1976: The effect of incorrect initial analysis on the predicted deepening of oceanic cyclones. *Preprints Sixth AMS Conf. Weather Forecasting and Analysis,* Albany, Amer. Meteor. Soc., 278–284.

——, and J. R. Gyakum, 1980: Synoptic–dynamic climatology of the "bomb." *Mon. Wea. Rev.*, **108**, 1589–1606.

Smith, R. K., 1980: Tropical cyclone eye dynamics. *J. Atmos. Sci.*, **37**, 1227–1232.

Staley, D. O., 1960: Evaluation of potential vorticity changes near the tropopause and the related vertical motions, vertical advection of vorticity, and transfer of radioactive debris from stratosphere to troposphere. *J. Meteor.*, **17**, 591–620.

——, and R. L. Gall, 1977: On the wavelength of maximum baroclinic instability. *J. Atmos. Sci.*, **34**, 1679–1688.

Tracton, M. S., 1973: The role of cumulus convection in the development of extratropical cyclones. *Mon. Wea. Rev.*, **101**, 573–593.

Weickmann, H. K., A. B. Long and L. R. Hoxit, 1977: Some examples of rapidly growing oceanic cumulonimbus clouds. *Mon. Wea. Rev.*, **105**, 469–476.

Yamasaki, M., 1968: Numerical simulation of tropical cyclone development with the use of primitive equations. *J. Meteor. Soc. Japan*, **46**, 178–201.